# Nonlinear Power Flow Control Design Methodology for Navy Electric Ship Microgrid Energy Storage Requirements

D.G. Wilson[1], PhD. ME, W.W. Weaver[2], PhD. EE, R.D. Robinett III[3], PhD AE, J. Young[4], Ph.D. OR, S.F. Glover[5], PhD. EE, M.A. Cook[6], MS CS, S. Markle[7] MS ME, T.J. McCoy[8], PhD. EE

[1]*R&D Controls Engineer, PI, Sandia Electric Ship Program, Sandia National Labs, Albuquerque, NM, USA; Corresponding Author, Email: dwilso@sandia.gov*
[2]*Professor, Power Electronics/Controls/Power System, Michigan Technological University, Houghton, MI, USA*
[3]*Professor, Nonlinear Controls & Optimization, Michigan Technological University, Houghton, MI, USA*
[4]*Chief Scientist, Nonlinear Optimization and Predictive Controls, OptimoJoe, LLC, Albuquerque, NM, USA*
[5]*R&D Manager, PM, Sandia Electric Ship Program, Sandia National Labs, Albuquerque, NM, USA*
[6]*R&D Software Engineer, Lead Agents/Informatics Controls, Sandia National Labs, Albuquerque, NM, USA*
[7]*Director Electric Ships Office PMS320 Program, NAVSEA, PMS 320, Washington, D.C., USA*
[8]*Former Director of Navy Electric Ship and Power Systems Expert, McCoy Consulting, Box Elder, ND, USA*

**Synopsis**

As part of the U.S. Navy's continued commitment to protecting U.S. interests at home and abroad, the Navy is investing in the development of new technologies that broaden U.S. warship capabilities and maintain U.S. naval superiority. NAVSEA is developing power systems technologies for the Navy to realize an all-electric warship. New nonlinear power system controls approaches are being developed to improve system performance in light of new electrically powered weaponry that behave as pulsed-loads. Advancements include the identification of pulsed-load profiles that identify Energy Storage System (ESS) requirements. A dynamic optimization engine has been developed and serves as the feedforward receding horizon control portion of the Hamiltonian Surface Shaping and Power Flow Control (HSSPFC) feedback controls for ESS networked microgrid system. A Coalition Warfare Program (CWP) test scenario was selected. The CWP is defined with a Reduced Order Model (ROM) that includes; generation, ESS, and mission pulsed-loads. Several numerical simulation studies were conducted. The CWP scenario is bounded by a baseline mission load local ESS contrasted with no ESS full nonlinear metastable boundaries. The main goal is to minimize ESS size and weight while maintaining power system performance. This paper focuses on the control and optimization of ESS as an integral part of supporting critical mission loads and real-time control algorithm development to improve future energy efficiency for multi-mission activities.

*Keywords:* Hierarchical control; Advanced Control; Energy Storage; Pulsed loads; Agent-based Control

## 1. Introduction

Future Navy electric ship system designs will require advanced power and energy storage systems that will require improved control, design and analysis techniques surrounding Medium Voltage DC (MVDC) power systems. The service power demands of these future naval warships may include the need for large amounts of power in short pulses from advanced sensors like high power radar, and future weapons such as railguns and lasers (Doerry, 2007). To support these pulsed power loads, response times for assistance from ESS must be shorter than what is currently available from the prime generation (Doerry, 2007). The goal of this project is to utilize advanced control design techniques (Robinett, 2011), (Wilson, 2014), (Wilson, 2015), (Weaver, 2016) to analyze ESS for Next Generation Integrated Power System Technologies (NGIPS), (Kuseian, 2013), (Neely, 2016). This enables open architectures, realize ESS requirements/devices, and create a design infrastructure to support the Navy and industrial research and development investments.

## 2. HSSPFC Three Tier Architecture

A nonlinear control design architecture based on HSSPFC employs both design trade-offs (off-line) and implementation of a three-tier realization (real-time). HSSPFC uses a power flow approach that balances generation and dissipation subject to stored power (kinetic and potential energies) which defines the Hamiltonian for the system. HSSPFC provides static stability conditions and identifies limit cycles as part of the dynamic stability conditions. Both necessary and sufficient conditions for stability are determined while allowing for performance specifications. Information theory concepts (information flow versus physical energy storage) are seamlessly integrated by including information kinetic and potential terms in the Hamiltonian definition. HSSPFC is not limited to conventional passivity control design and utilizes energy shaping techniques, inherent in the

Hamiltonian surface, to provide a sense of static stability.  Many conventional nonlinear control designs in the field are unaware of the surface shaping and its relationship to static stability.

An advanced control architecture that shows the HSSPFC (Wilson, 2014), (Wilson, 2016a), tertiary information flow and the Hamiltonian energy storage integration level is given in Figure 1. A dynamic optimization planner, based on the Optizelle (Young, 2014) toolset, is utilized for the guidance controls block. The informatics/agent based architecture relies on Optizelle for ESS optimizations. Given generation and load estimates, set points are generated to feed into both the Hamiltonian energy storage controller and the servo controller levels. Within each level of the architecture, the communication bandwidth and sample frequencies increase with the criticality of the information flow.
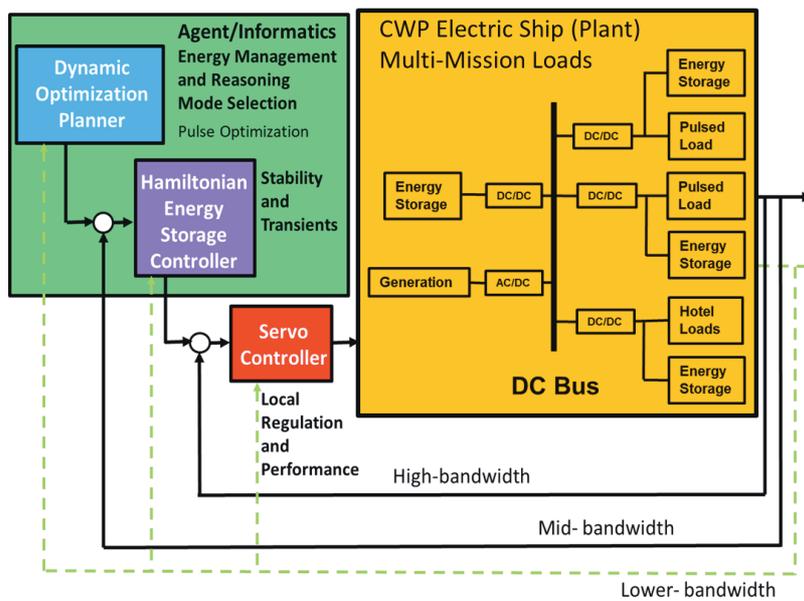


Figure 1: HSSPFC three tier architecture for CWP electric ship with multi-mission loads

### 2.1.    *CWP Electric Ship Multi-Mission Loads Plant Model*

This section introduces a ROM for a single DC microgrid with generation, generic energy storage on the bus Energy Magazine (EM), and a single mission pulsed-load (Solid State Laser, SSL) combined with a hotel load (see Figure 2), respectively. The main objective is to be able to define control methodologies that minimize ESS. Specifically, the HSSPFC design methodology is applied to evaluate ESS to support mission pulsed-loads.
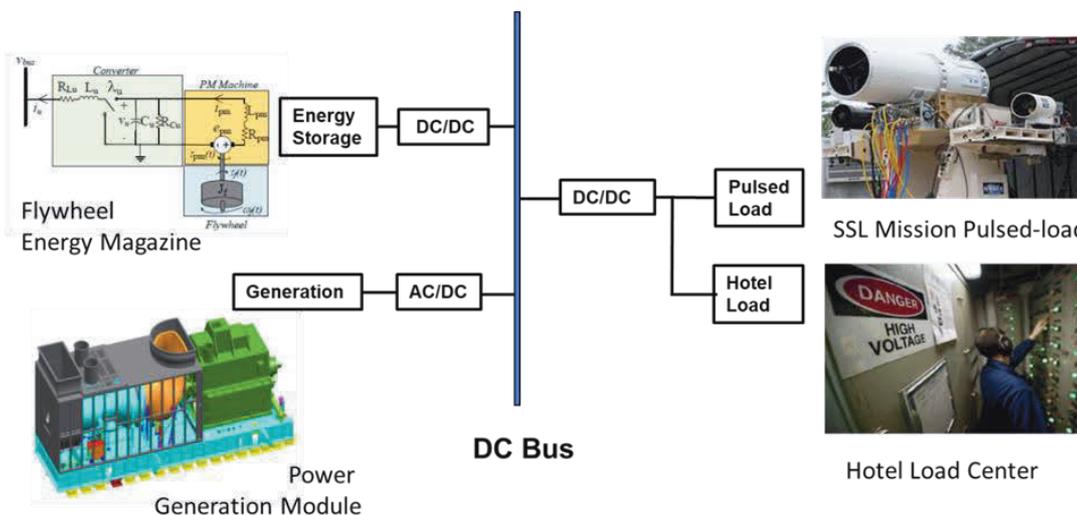


Figure 2: ROM for HSSPFC control design

### 2.2.    *Agent Informatics Energy Management and Reasoning Mode Selection*

The first layer is agent/informatics energy management and reasoning mode selection (see Figure 1, green). This layer includes a guidance algorithm that is updated based on steady-state set-points that are determined from a dynamic optimization planner.  The update rate is on the order of seconds typically provided by an ethernet communication network.

The agent informatics component of the advanced control architecture performs energy management by monitoring and influencing the state of the electrical system. The microgrid module electrical system has been instrumented with sensors to mainly monitor voltage and current. The power management agent monitors a high tempo flow of sensor measurements in order to model the electrical system state. An optimization engine is called periodically with current and possible electrical system states in order to determine the best microgrid component set points. The power management agent translates the optimization results into control actions that result in update commands to the electrical system.

The power management agent communicates with Optizelle and the electrical system periodically to control the electrical system. The agent formulates optimization input problems for Optizelle to solve using a predefined JavaScript Object Notation (JSON) format. The problem statement defines the optimization objectives and characteristics of the electrical system, such as the bus configuration, connected components, component values with initial conditions.  The agent interprets Optizelle output JSON formatted solutions for the suggested set points of microgrid components. The diagram in Figure 3 shows the main interaction between the power management agent and the electrical system. A power management agent may be customized to collaborate with peer software agents. The multi-agent system has been tailored to fit the Secure Scalable Microgrid Testbed (SSMTB) (Glover, 2011) defined electrical system and communication protocol.
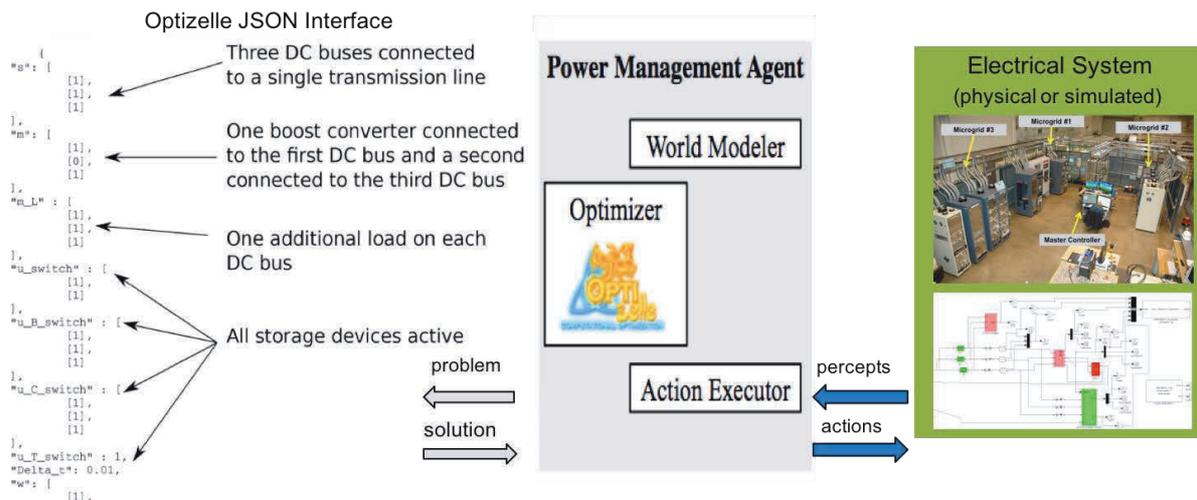


Figure 3: Agent informatics energy management and reasoning flow diagram

### 2.3.    *Dynamic Optimization Planner*

The dynamic optimization planner is an optimal control algorithm based on an on-line optimization engine that solves for a receding-horizon control. On-line means that it solves for a new control while the system is in operation.  This is necessary because the algorithm executes in a variable amount of time since it is based on a nonlinear optimization formulation.  In general, a solution time is only deterministic for linear-quadratic control formulations.  The solution it finds is a receding horizon control where the control is based on a prediction of the operating system (planning horizon) (Young, 2017) and is executed as long as the prediction remains accurate (execution horizon).

The optimal control problem can be formulated as a microgrid circuit (CWP) comprised of three components: boost converter, DC buses, and connectors.  These components along with their parameters are shown in Figure 4.  The Optizelle library (Young, 2014) and modularization allows for quick formulation of new topologies.  The optimizer is called by the agent/informatics portion with updated ESS allocation cost function weights (see Figure 1, light blue).
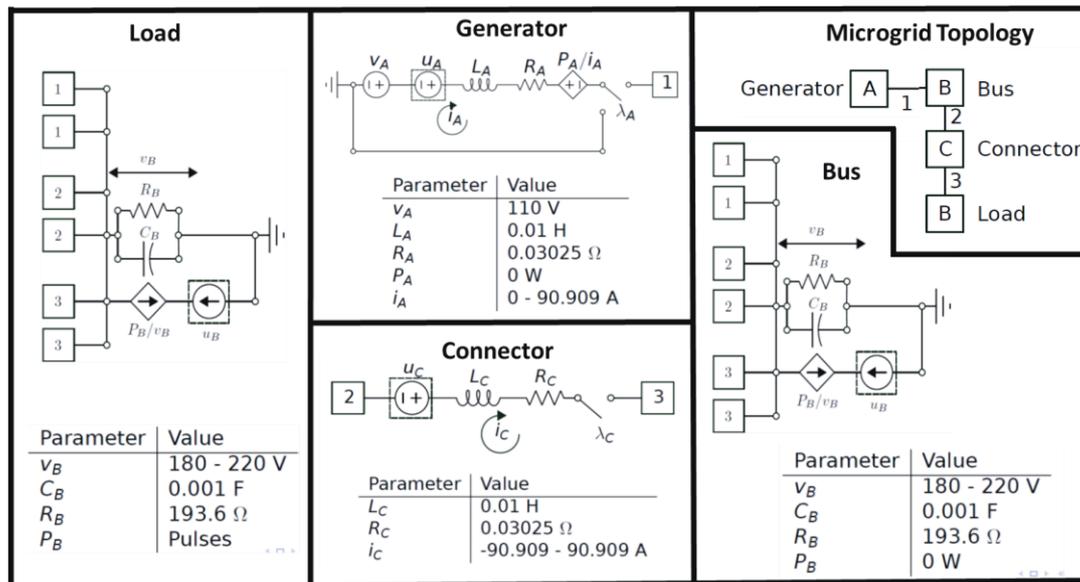
Figure 4: Optizelle library components and parameters with selected topology for CWP microgrid configuration

### 2.4.    *HSSPFC Energy Storage Controller*

The second layer is the energy storage HSSPFC controller (see Figure 1, purple) which provides system stability and transient performance.  The update rate can be on the order of milliseconds and uses both network communication and hardwired feedback loops.  HSSPFC has been developed for microgrid systems in general and currently includes; i) a single DC Microgrid, ii) networked DC microgrids (Weaver, 2015a, 2015b), iii) AC single/networked inverter-based microgrids (Wilson 2016b), iv) AC inverter/synchronous generator microgrids, vi) hybrid AC/DC individual/networked microgrids (Wilson, 2018), and vii) multi-spinning machines on an AC bus (Matthews, 2018).  Several conditions are investigated; i) ESS optimization for controller set-points, ii) baseline ESS requirements for a single mission load under steady-state conditions, and iii) nonlinear metastable boundaries with no ESS.  This captures the trade space available for ESS design with respect to all electric warship assessments.

### 2.5.    *Servo Controller*

The third layer is the servo level (see Figure 1, red) which operates the boost converters as servo systems at the fastest update rates which are on the order of microseconds.  The servo loops are hardwired with tight timing loops directly in conjunction with the hardware components and accept set-points from the other control layers.

### 3.  Contrasting Bus and Load ESS Optimization Agent/Informatics Based Selections

The optimal formulation is configured to minimize: i) use of ESS devices, ii) changes in boost converter duty cycles, iii) parasitic losses, and iv) power used by ESS devices.  The cost function is subject to: i) boost converter state equations, ii) DC bus state equations, iii) DC to DC bus state equations, iv) other AC/DC components, v) power/energy terms, vi) differential equation discretization, and vii) bounds on voltages, currents, duty cycles, etc.

The dynamic optimizer is utilized to contrast two optimization scenarios that demonstrate ESS with an emphasis on reducing load storage (Case 1) or EM bus storage (Case 2), respectively. The optimizer, by changing the weighting in the ESS locations, produced the control set points for each of these scenarios. This allows the agent/informatics control layer to reconfigure and select ESS based on availability or state-of-charge status. ESS is available in general; i) at the generator, ii) at the load, iii) on the DC bus EM, and iv) connectors (see Figure 4).

Both cases support an SSL mission load characterized as two 12 kW pulses (see Figure 5).  For Case 1 ESS use is minimized with a penalty on load ESS.  The generator is assumed to be at full capacity and resulted in reduction in ESS on the *load* for both power (see Figure 6 a) and energy (see Figure 6 b) consumed. For Case 2 ESS use is minimized with a penalty on bus EM ESS.  The generator is assumed to be at full capacity and resulted in reduction in ESS on the *bus* EM for both power (see Figure 6 c) and energy (see Figure 6 d) consumed.
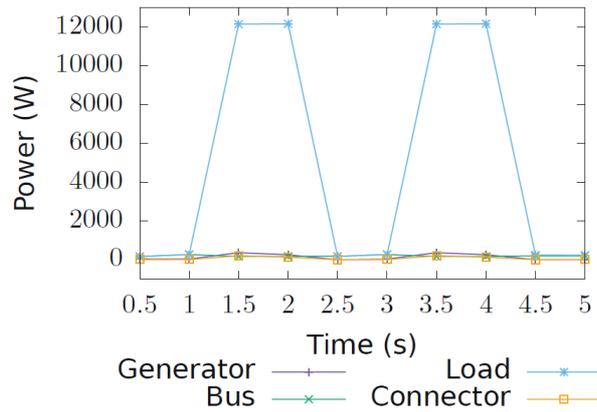
Figure 5: 12 kW pulses, ESS everywhere with penalties according to Cases 1 and 2
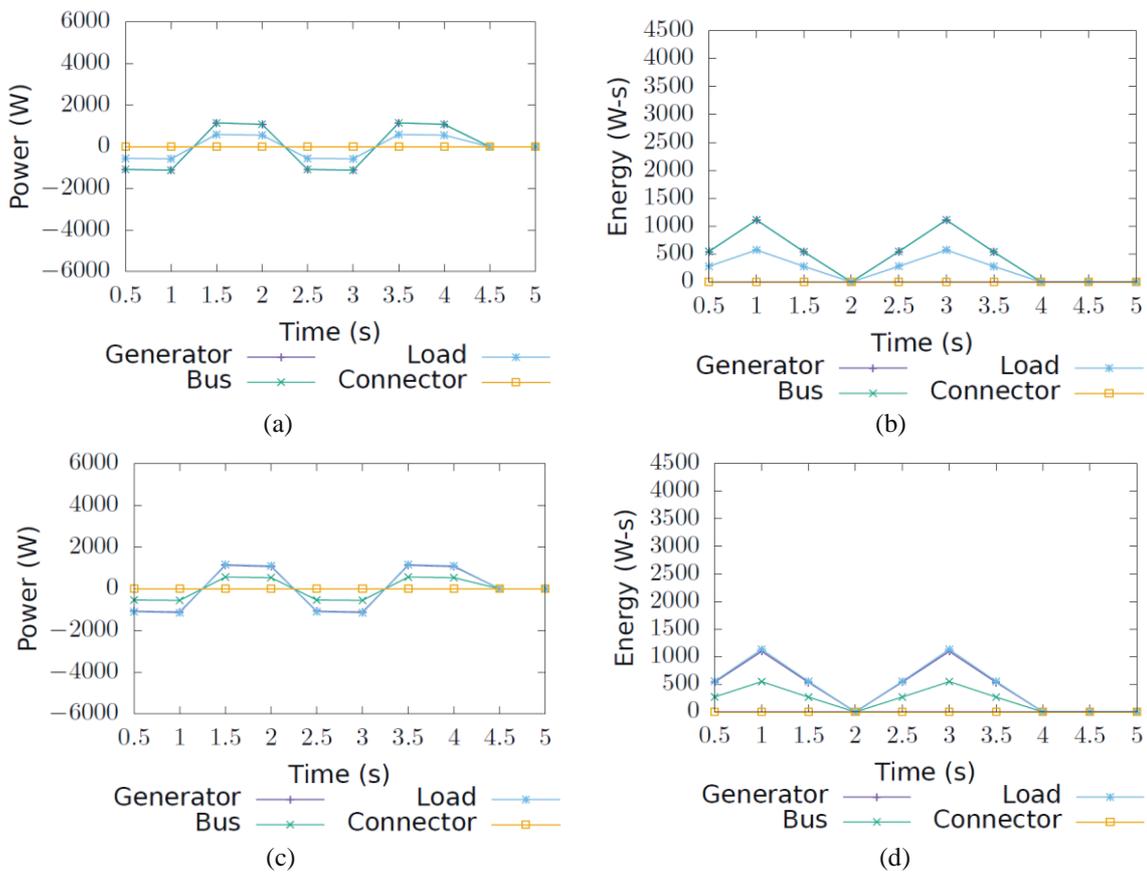


Figure 6: 12 kW pulses – power (a) and energy (b) used by ESS with penalty on load storage; power (c) and energy (d) used by ESS with penalty on bus storage

## 4. Baseline ESS Design Approach for Single Mission Load

For a typical power system approach the *design criteria* includes: i) the bus voltage remains constant, ii) all loads are satisfied when energy and power are needed, and iii) the system is stable from a linear systems perspective. To satisfy the *design criteria* the design approach must: i) place sufficient ESS local to each pulsed load to service that load and ii) implement linear controls that operate within the linear stability boundary.

### 4.1.    *Single DC Microgrid with ESS and Mission Load ROM Configuration*

The circuit schematic and relevant dynamics for the ROM single DC microgrid with mission pulsed-load that includes ESS (ideal controllers) at the generator ($u_1$), EM bus ($u_5$), and pulse load A ($u_2$) as shown in Figure 7. The SSL pulsed-load and hotel load are given as $P_2(t)$.
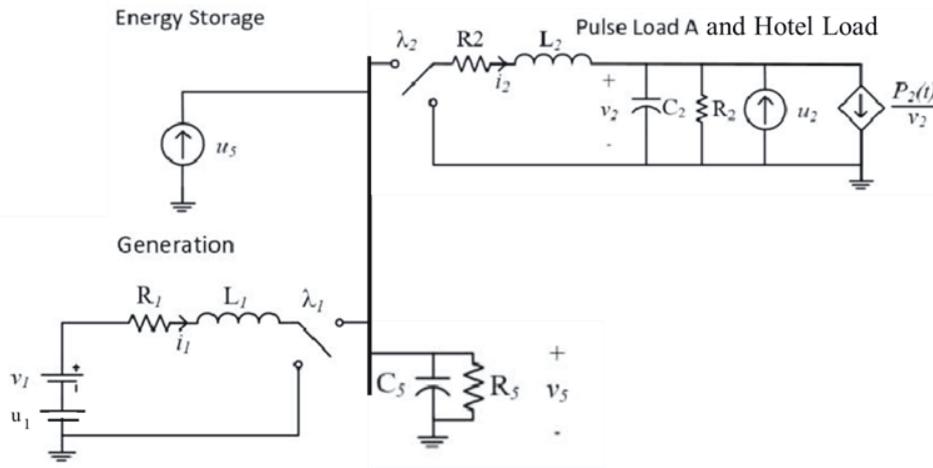


Figure 7: Electrical circuit schematic for single DC microgrid with single mission pulsed-load

The system circuit equations are determined for the boost converters and bus voltages as

$$L_1 \frac{di_1(t)}{dt} = -R_{L1}i_1(t) - \lambda_1 v_5(t) + v_1 + u_1$$

$$L_2 \frac{di_2(t)}{dt} = -R_{L2}i_2(t) + \lambda_2 v_5(t) - v_2(t)$$

$$C_2 \frac{dv_2(t)}{dt} = i_2(t) - \frac{P_2(t)}{v_2(t)} - \frac{v_2(t)}{R_2} + u_2$$

$$C_5 \frac{dv_5(t)}{dt} = \lambda_1 i_1(t) - \lambda_2 i_2(t) - \frac{v_5(t)}{R_5} + u_5$$

.

(1)

The system circuit equations are assembled in matrix form as

$$M\dot{x} = Rx + f(x,u,t) + D^T v + B^T u$$
$$= \left[\overline{R} + \tilde{R}\right]x + f(x,u,t) + D^T v + B^T u$$

(2)

where the matrix and parameter definitions are given in the Appendix. The PI controllers for **u** have been designed in previous work (Wilson, 2016a)**,** (Wilson, 2014) which includes the stability conditions, respectively. For this investigation only, the ideal ESS for the EM bus control is employed to determine the reference current required for the flywheel ESS device. The next subsection determines the actual ESS requirements to meet the mission pulsed-load. The mission pulsed-load is modeled after the SSL mission load and scaled for the SSM flywheel model.

### 4.2.    *Baseline Comparison: want ESS Device to Supply all Non-DC Energy*

For the baseline ESS design the focus is on the pulsed load A circuit (see Figure 7) that follows the *design criteria* where it is desired that $u_2$ supplies all the non-DC energy. The *design approach* can further be described by the following steps:
   **Step 1:** Given specifications (operating condition determined from mission pulsed load profile)
   **Step 2:** Design ESS that meets given specifications:
        1)   ESS devices with specifications,
        2)   ESS model specifications,
        3)   ESS model parameter characteristics,

4) Integrate multiple ESS devices if necessary,
5) Evaluate ESS to meet mission pulsed-load.

For Step 1, the SSL mission pulsed-load power profile specification is shown in Figure 8 (blue). Decomposition of the mission pulsed load profile identifies the generator specification with a 2.5 kW minimum required generator power (see Figure 8, green). The mission pulse component is shown in Figure 8 (gold). The AC component of the pulse is the ESS specification (Figure 8, red). The maximum power and energy requirements can be determined from one pulse cycle of the load. The maximum power specification shown in Figure 9 is 1.025 kW. The maximum or peak energy specification shown in Figure 10 is 163.54 J. By performing a PSD on the pulsed-load profile the ESS frequency bandwidth requirement is 50 Hz as shown in Figure 11. The bandwidth of a *candidate* ESS device will need to meet this frequency spectrum. The ESS device needs to be able to *provide* a minimum storage capacity of 163.54 J to meet the pulsed-load profile. However, the actual storage hardware device specifications will be determined by the round-trip efficiency and minimum energy storage requirements of the chosen ESS device.

For Step 2, a list of *candidate* ESS devices are reviewed (i.e., flywheels, capacitors, batteries, etc.). The ESS sizing is determined from the maximum power and energy specifications. A closed loop Bode plot determines the frequency characteristics which are contrasted with the specifications from Step 1. For purposes of this example, a ESS flywheel system is selected.
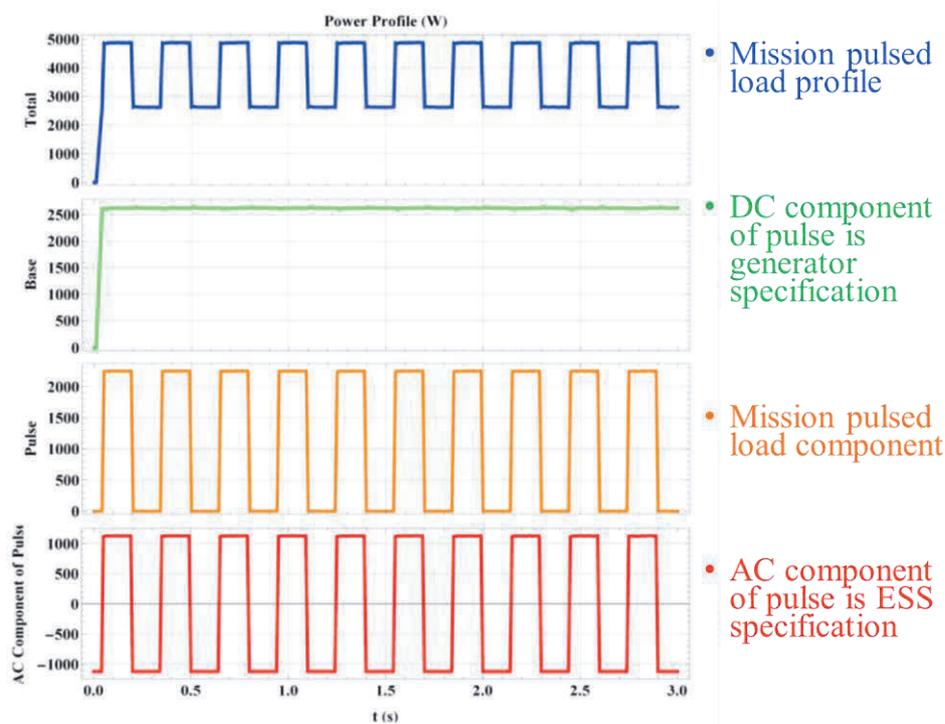


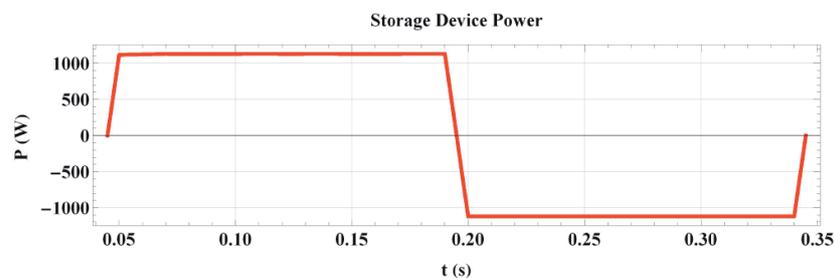Figure 8: ESS device only needs to provide AC component (bottom plot)



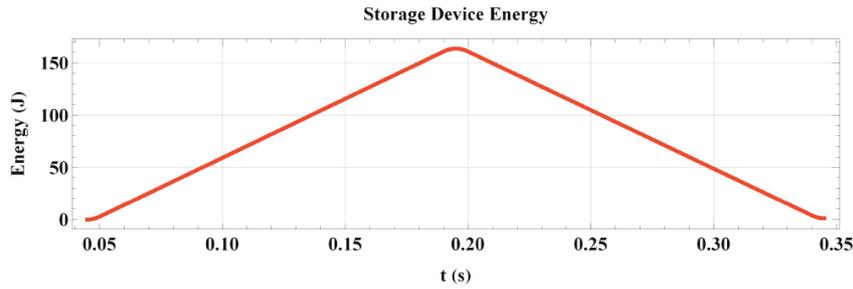Figure 9: One cycle of the power from the ESS device

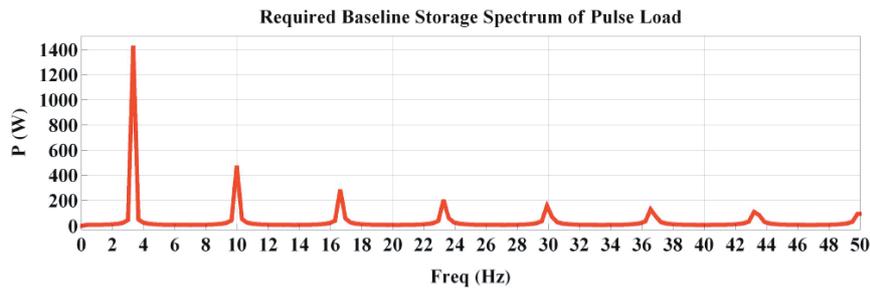Figure 10: Integrating power gives the energy in the ESS device



Figure 11: Baseline frequency component specification for an ideal ESS device for load

### 4.3.  Servo-Mode Monolithic Flywheel ESS Model

Next a monolithic ESS reduced order servo-mode flywheel model is developed (see Figure 12). This model contains a spinning mass flywheel, permanent magnet (PM) DC machine and a DC-DC converter to interface with the microgrid bus. This reduced order model does include parasitic components to emulate the efficiency losses in the real hardware, including electrical resistive losses and mechanical friction losses which also contribute to damping and bandwidth response limitations. The ideal ESS reference profiles from the previous model (see Figure 7) will be employed as a reference signal to evaluate the tracking and performance characteristics.
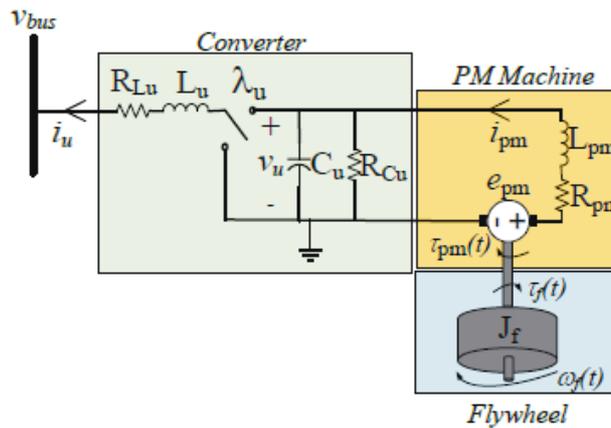


Figure 12: Monolithic flywheel ESS and servo-mode system

The reduced order flywheel modeling assumptions are:

1.  Converter model is average mode with control input duty cycle ($\lambda_u$).  Switching effects are ignored.
2.  The electrical machine used is a permanent magnet DC machine for simplicity and reduced order. Typically, this machine would be a 3-phase induction machine, permanent magnet synchronous AC machine or potentially a switched reluctance machine.

3. The minimum speed of the flywheel will be such to support a voltage $e_{pm} = k_t \omega_f(t) \geq v_{bus}$ $\forall$ t. Therefore, a buck converter (in source mode as shown below where $v_u > v_{bus}$) is used as the bus interface.
4. The energy stored is

$$W_f = \tfrac{1}{2} J_f \omega_f(t)^2.$$

(3)

Therefore, the minimum energy stored in the device is

$$W_{f,\min} = \tfrac{1}{2} J_f \left(\tfrac{v_{bus}}{k_t}\right)^2.$$

(4)

5. The power losses in the device are

$$P_{loss} = R_{pm} i_{pm}(t)^2 + R_{Lu} i_u(t)^2 + \tfrac{v_u(t)^2}{R_{Cu}} + B \omega_f(t)^2.$$

(5)

The flywheel is modeled as

$$J_f \omega_f'(t) = -B \omega_f(t) - k_t i_{pm}(t)$$

(6)

where B is the friction coefficient, $k_t$ is the torque constant and the torque is found from $\tau_{pm} = k_t i_{pm}(t)$ in the permanent magnet (PM) machine. The PM electrical machine model is

$$L_{pm} i_{pm}'(t) = k_t \omega_f(t) - R_{pm} i_{pm}(t) - v_u(t)$$

(7)

where $k_t \omega_f(t)$ is the speed voltage generated by the mechanical moment. The DC-DC converter is model as

$$C_u v_u'(t) = -\tfrac{v_u(t)}{R_{Cu}} + i_{pm}(t) - \lambda_u i_u(t)$$
$$L_u i_u'(t) = -v_{bus} - R_{Lu} i_u(t) + \lambda_u v_u(t)$$

(8)

Then the overall flywheel ESS model becomes

$$J_f \omega_f'(t) = -B \omega_f(t) - k_t i_{pm}(t)$$
$$L_{pm} i_{pm}'(t) = k_t \omega_f(t) - R_{pm} i_{pm}(t) - v_u(t)$$
$$C_u v_u'(t) = -\tfrac{v_u(t)}{R_{Cu}} + i_{pm}(t) - \lambda_u i_u(t)$$
$$L_u i_u'(t) = -v_{bus} - R_{Lu} i_u(t) + \lambda_u v_u(t)$$

(9)

The flywheel equivalency to the generalized idealized ESS model is given by

$$i_u(t) = u_b.$$

(10)

This model can be assembled into matrix notation similar to (2). A simple PI control on the current injection is determined as

$$\tilde{x} = i_{u,\text{ref}} - i_u(t)$$
$$\tilde{x}_i'(t) = \tilde{x}$$
$$\lambda_u = k_i \tilde{x}_i + \tilde{x} k_p$$
$$0 \leq \lambda_u \leq 1$$

(11)

Then the combined system model with controls becomes

$$J_f\,\omega_f{}'(t) = -\,B\,\omega_f(t) - k_t\,i_{\mathrm{pm}}(t)$$

$$L_{\mathrm{pm}}\,i_{\mathrm{pm}}{}'(t) = k_t\,\omega_f(t) - R_{\mathrm{pm}}\,i_{\mathrm{pm}}(t) - v_u(t)$$

$$C_u\,v_u{}'(t) = -\,i_u(t)\left(k_i\,\tilde{x}_i(t) + k_p\left(i_{u,\mathrm{ref}} - i_u(t)\right)\right) - \frac{v_u(t)}{R_{\mathrm{Cu}}} + i_{\mathrm{pm}}(t)$$

$$L_u\,i_u{}'(t) = v_u(t)\left(k_i\,\tilde{x}_i(t) + k_p\left(i_{u,\mathrm{ref}} - i_u(t)\right)\right) - v_{\mathrm{bus}} - R_{\mathrm{Lu}}\,i_u(t)$$

$$\tilde{x}_i{}'(t) = i_{u,\mathrm{ref}} - i_u(t)$$

(12)

This monolithic flywheel model was utilized to evaluate the idealized ESS reference signal, representing the EM bus ESS, derived in Section 4.2 and evaluated in Section 4.4. The scaled parameters, based on SSMTB hardware, for this flywheel system are given in the Appendix Table 1. For this example, only a single monolithic flywheel ESS is selected.

### 4.4.    *Evaluate Flywheel ESS to Meet Mission Pulsed-load and Assess Performance*

The HSSPFC design methodology was evaluated to assess the performance of the flywheel energy storage model with respect to the idealized energy storage system requirements. The pulse-load profile from Section 4.2 was employed (see Figure 8, blue). Other results that include the bus voltage, power required for the energy storage, commanded actual flywheel currents, and flywheel current errors are shown in Figure 13 to Figure 17, respectively. The flywheel ESS device tracks the required or ideal energy storage command to support the mission pulsed load requirement (see Figure 15 and Figure 16, respectively).
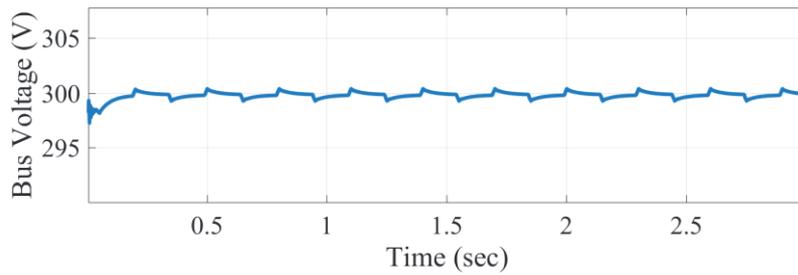


Figure 13: DC bus voltage regulated to +/- 5% nominal
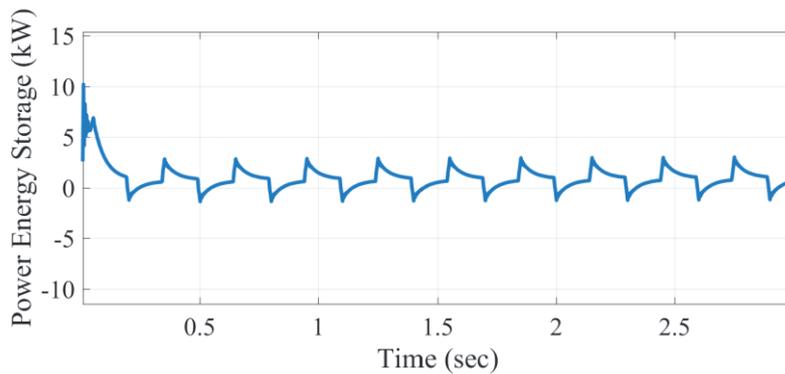


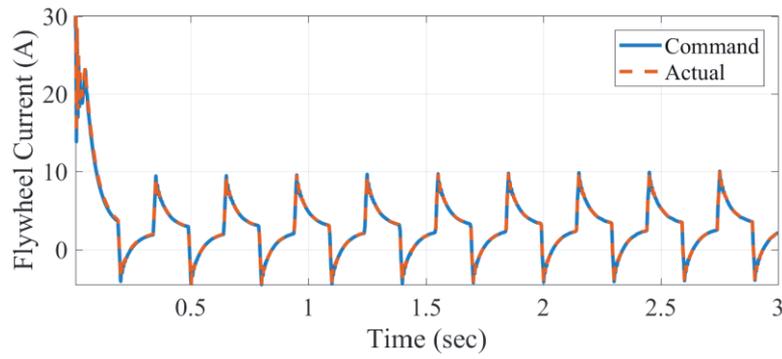Figure 14: EM bus ESS power profile
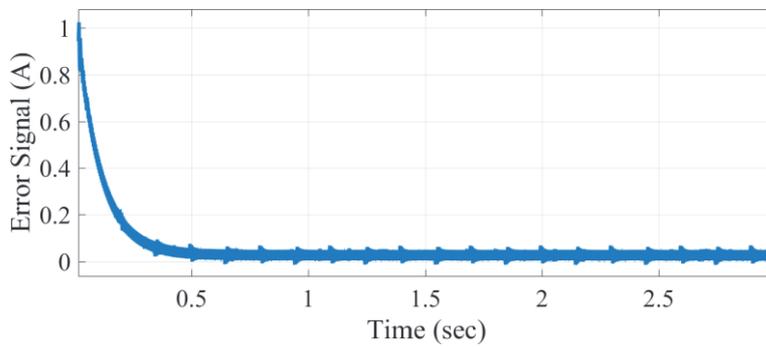
Figure 15: Command flywheel and actual flywheel current



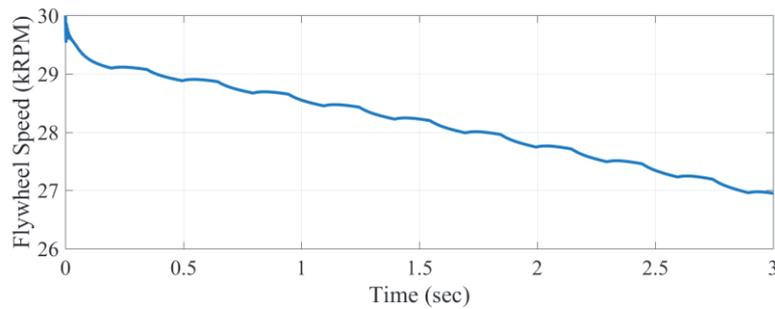Figure 16: Command flywheel and actual flywheel error signal



Figure 17: Flywheel speed profile

### 4.5. Closed Loop Bode Plot analysis

A closed loop Bode plot helps to determine the frequency characteristics and can be used to contrast with the specifications and requirements. The monolithic flywheel, given in (12), can be linearized with input of $i_{ref}$ and output of $i_u$ determined as:

$$\begin{pmatrix} -\dfrac{B}{J_f} & -\dfrac{k_t}{J_f} & 0 & 0 & 0 & 0 \\[2mm] \dfrac{k_t}{L_{pm}} & -\dfrac{R_{pm}}{L_{pm}} & -\dfrac{1}{L_{pm}} & 0 & 0 & 0 \\[2mm] 0 & \dfrac{1}{C_u} & -\dfrac{1}{C_u R_{Cu}} & 0 & 0 & 0 \\[2mm] 0 & 0 & 0 & -\dfrac{k_p\,v_{uo}+R_{Lu}}{L_u} & \dfrac{k_i\,v_{uo}}{L_u} & \dfrac{k_p\,v_{uo}}{L_u} \\[2mm] 0 & 0 & 0 & -1 & 0 & 1 \\[2mm] 0 & 0 & 0 & 1 & 0 & 0 \end{pmatrix}^{\!s}$$

(13)

The transfer function becomes:

$$G(s) = \frac{i_u}{i_{ref}} = -\frac{v_{uo}\,(s\,k_p+k_i)\,\big((B+s\,J_f)\,(s\,L_{pm}\,(s\,C_u\,R_{Cu}+1)+s\,C_u\,R_{Cu}\,R_{pm}+R_{Cu}+R_{pm})+k_t^2\,(s\,C_u\,R_{Cu}+1)\big)}{(v_{uo}\,(s\,k_p+k_i)+s\,(s\,L_u+R_{Lu}))\,(R_{Cu}\,(-(B+s\,J_f))-(s\,C_u\,R_{Cu}+1)\,((B+s\,J_f)\,(s\,L_{pm}+R_{pm})+k_t^2))}$$

(14)

The Bode plot of this transfer function, shown in Figure 18, utilizes the parameters from Table 1. The roll-off frequency is about 10 kHz (60 krad/sec point on plot). This would easily meet the 50 Hz design requirement established with the baseline PSD frequency calculations. In practice, a hardware implementation would likely have switching at 10kHz. A well-built power electronics hardware design would probably have a frequency response about 10x less than the Bode prediction, or closer to 1kHz which is within the ESS specifications.
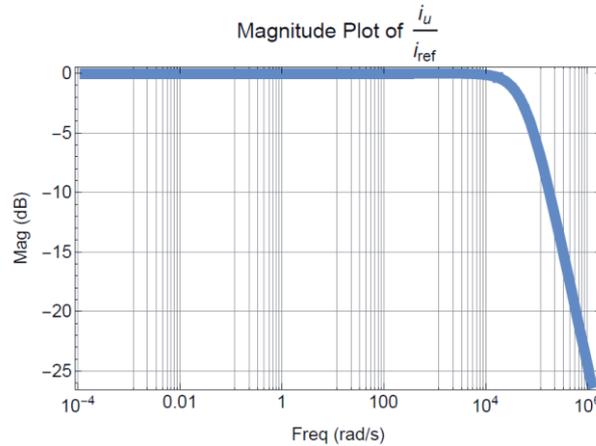


Figure 18: Flywheel ESS transfer function Bode plot response

## 5.  The Advanced Power System Design Approach

The *design criteria* for the bounding stability case includes: i) the bus voltage allowed to vary, ii) all loads are satisfied when energy and power are needed, and iii) the system is stable from a *nonlinear* system perspective. This design approach highlights nonlinear controls advantages that include: i) elimination of all ESS and ii) implementation of controls that operate within the nonlinear stability boundary (Weaver, 2017). From (Weaver, 2017) both Floquet and HSSPFC techniques show the same region of constant power stability (where $D_p$ is the percent duty cycle and P is power). However, HSSPFC shows a lower prediction region of *meta-stability* (see Figure 19 solid black line). The limiting design cases are all (see earlier baseline discussion) or none. None implies that the source can supply all loads and no additional ESS is needed.
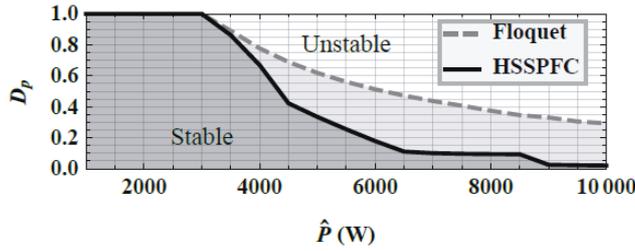
Figure 19: HSSPFC and Floquet stability boundaries (with $T_p$ = 0.5 sec)

The *meta-stability* HSSPFC boundary for the CWP test scenario microgrid system is shown in Figure 20 (left), where the surface represents the maximum stable (meta-stable) limit cycle behaviour of the bus voltage. This 3D surface represents the upper no-ESS condition.
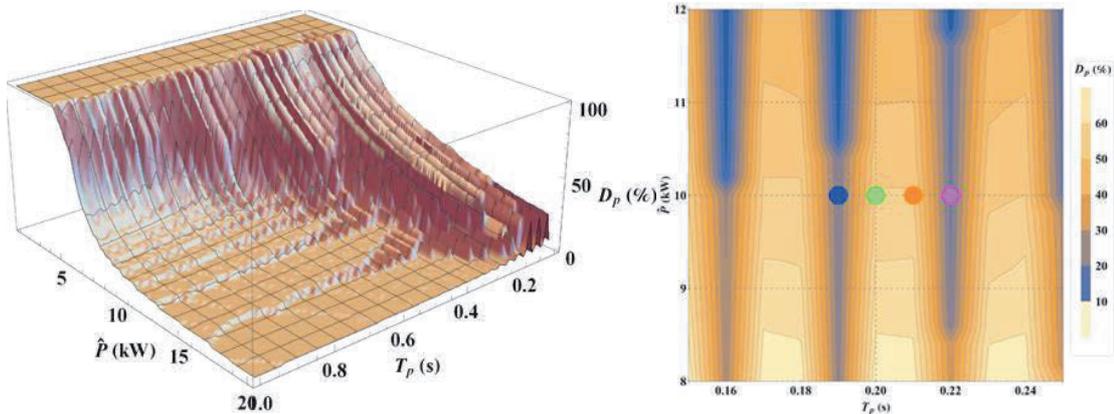


Figure 20: Meta-stability boundary CWP test scenario microgrid system (left) and cross-section map (right)

To verify the *meta-stability*, four points on the map were selected and simulations were run to check. Figure 20 (right) shows the four Cases on the map and the corresponding time domain simulations results (see Figure 21) of $P_2$, $v_2$ and $v_5$ (color-coded). Also, included in the plots are the cut-off lines (gray) for the voltages to be determined as "unstable." In the first and last cases (blue, magenta) the $v_2$ voltage hits the stability line and ends the simulation.
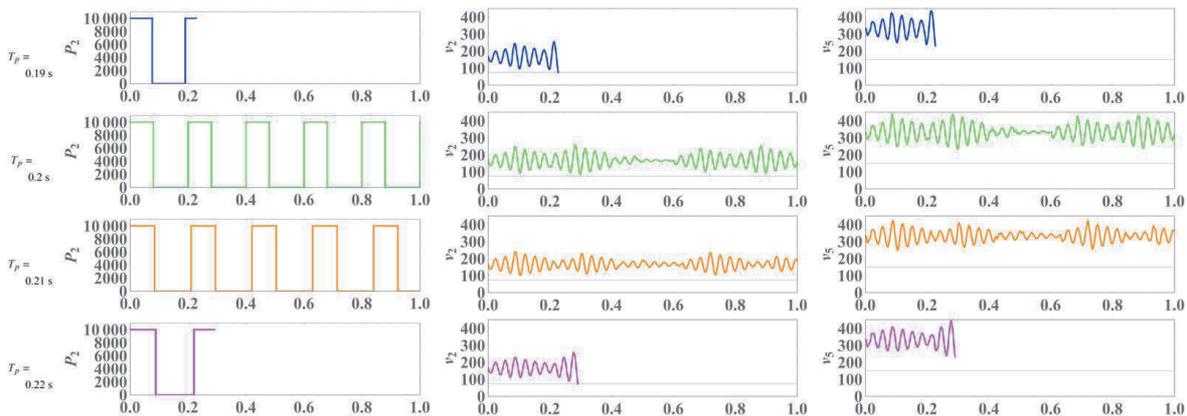


Figure 21: Meta-stability time domain simulation results (color-coded)

## 6.    Conclusions

The main goal of this investigation was to minimize ESS size and weight while maintaining power system performance.  The paper focused on the control and optimization of ESS as an integral part of supporting critical mission loads with advanced control algorithm development to improve future energy efficiency for multi-mission Navy all electric warship activities.

## 7.  Acknowledgements

## 8.  References

Doerry, N., Next Generation Integrated Power System NGIPS Technology Development Roadmap, Naval Sea Systems Command, Washington, D.C., Ser. 05D/349, 30 Nov. 2007.

Glover, S. and Robinett III, R.D., Enabling Secure, Scalable Microgrids with High Penetration Renewables, Grand Challenge LDRD, SAND2011-0935P, 2011.

Kuseian, J., "Naval Power Systems Technology Development Roadmap PMS 320," Naval Sea Systems Command, Washington, D. C., April 2013.

Matthews, R.C., Weaver, W.W., Robinett III, R.D., and Wilson, D.G., Hamiltonian Methods of Modeling and Control of AC Microgrids with Spinning Machines and Inverters, *International Journal of Electrical Power and Energy Systems*, 98(2018) 315-322.

Neely, J., Rashkin, L., Cook, M., Wilson, D.  and Glover, S., "Evaluation of Power Flow Control for an All-Electric Warship Power System with Pulsed Load Applications," in APEC 2106, Long Beach Convention & Entertainment Center, Long Beach, CA, 2016.

Robinett III, R.D. and Wilson, D.G., Nonlinear Power Flow Control Design:  Utilizing Exergy, Entropy, Static and Dynamic Stability, and Lyapunov Analysis, Springer-Verlag London Ltd., August 2011, ISBN 978-0-85729-822-5.

Weaver, W.W., Robinett III, R.D., Wilson, D.G. and Matthews, R.C., "Meta-Stability Control of Pulse Power Loads using the Hamiltonian Surface Shaping Method," in *Special Topics Journal on Electric Ship, IEEE Transactions on Energy Conversion*, DOI 10.1109/TEC.2017.2652980, January 2017.

Weaver, W. W., Robinett III, R.D., Parker, G. and Wilson, D.G., "Distributed Control and Energy Storage Requirements of Networked DC Microgrids," *Control Engineering Practice*, vol. 44, pp. 10-19, 2015.

Weaver, W.W., Robinett III, R.D., Parker, G. G. and Wilson, D.G., "Energy Storage Requirements of DC Microgrids with High Penetration Renewables Under Droop Control," *International Journal of Electrical Power and Energy Systems*, vol. 68, pp. 203-209, 2015.

Wilson, D.G., Cook, M. A., Neely, J., Glover, S. F. and Rashkin, L., "Nonlinear Power Flow Control Design for NGIPS Energy Storage Requirements, Phase I," Sandia Report SAND2016-1873, February 2016 revised.

Wilson, D. G., Neely, J., Cook, M. Glover, S., Young, J. and Robinett III, R. D., "Hamiltonian Control Design for DC Microgrids with Stochastic Sources and Loads with Applications," *International Symposium on Power Electronics, Electrical Drives, Automation and Motion*, SPEEDAM 2014, Ischia, Italy.

Wilson, D., Robinett III, R. D., Weaver, W., Byrne, R. and Young, J., "Nonlinear Power Flow Control Design of High Penetration Renewable Sources for AC Inverter Based Microgrids," *International Symposium on Power Electronics, Electrical Drives, Automation and Motion*, SPEEDAM 2016, AnaCapri, Capri Island, Italy.

Wilson, D.G., Weaver, W.W., Robinett III, R.D., Glover, S.F., "Nonlinear Power Flow Control Design for Networked AC/DC based Microgrid Systems," *2018 IEEE American Control Conference*, Milwaukee, WI, June 27-29, 2018.

Young, J., Optizelle: An open source software library designed to solve general purpose nonlinear optimization problems, 2014, www.optimojoe.com, Open source software.

Young, J., Cook, M.A., Wilson, D.G., A Predictive Engine for On-Line Optimal Microgrid Control, *2017 IEEE Electric Ship Technologies Symposium, ESTS 2017*, February 2017, Arlington, Virginia, August 15-17, 2017.

## 9. Appendix

Where the state is

$$x^T = \begin{bmatrix} i_1(t) & i_2(t) & v_2(t) & v_5(t) \end{bmatrix}$$

(15)

and the matrix definitions are given as

$$M = diag[L_1 \quad L_2 \quad C_2 \quad C_5]$$

(16)

$$R = \begin{bmatrix} -R_{L1} & 0 & 0 & -\lambda_1 \\ 0 & -R_{L2} & -1 & \lambda_2 \\ 0 & 1 & -\dfrac{1}{R_2} & 0 \\ \lambda_1 & -\lambda_2 & 0 & -\dfrac{1}{R_5} \end{bmatrix} \quad f(x,u,t) = \begin{bmatrix} 0 \\ 0 \\ -\dfrac{P_2(t)}{v_2(t)} \\ 0 \end{bmatrix} \quad u = \begin{bmatrix} u_1 \\ u_2 \\ u_5 \end{bmatrix} \quad v = [v_1]$$

(17)

$$D^T = \begin{bmatrix} 1 \\ 0 \\ 0 \\ 0 \end{bmatrix} \quad B^T = \begin{bmatrix} 1 & 0 & 0 \\ 0 & 0 & 0 \\ 0 & 1 & 0 \\ 0 & 0 & 1 \end{bmatrix}$$

(18)

Note symbols:  L inductors, R resistors, C capacitors, v voltages, u ESS controls, $P_2(t)$ pulsed power load input, and $\lambda$ are the converter duty cycles.

Table 1: Scaled flywheel parameters

| Parameter | Description | Value |
|---|---|---|
| $J_f$ | Moment of Inertia | $0.00354 \, Kg \, m^2$ |
| $k_t$ | Torque Constant (flux – linkage) | $0.229 \, Nm / A$ |
| $R_{pm}$ | Armature Resistance | $0.1266 \, \Omega$ |
| $L_{pm}$ | Armature Inductance | $0.4457 \, mH$ |
| $C_u$ | Converter Capacitance | $1000 \, \mu F$ |
| $R_{Cu}$ | Converter Resistance | $10 \, K\Omega$ |
| $L_u$ | Line Inductance | $10 \, mH$ |
| $R_u$ | Line Resistance | $0.1 \, \Omega$ |
| B | Shaft Windage | $1.17 \, E - 06 \, Nm \big/ \frac{rad}{s}$ |
| $v_{bus}$ | Nominal Bus Voltage | $300 \, V$ |
| Max Speed | | $37\,500 \, RPM \ = 3927 \, rad / s$ |
| Max Energy | | $27\,254.1 \, J$ |
| Min Speed | | $12\,500 \, RPM \ = \ 1309 \, rad / s$ |
| Min Energy | | $3033 \, J$ |